Electronic Supplementary Information for

Enhancing SIM behaviour in a mononuclear tetrahedral [Co(N,N'-2-iminopyrrolyl)₂] complex

Patrícia S. Ferreira,[a,b] José F. Malta,[b,c] Nuno A. G. Bandeira,*[d] Alexander Allgaier,[e] Joris van Slageren,*[e] José A. Paixão,[c] Manuel Almeida,[b] Laura C. J. Pereira,*[b] Pedro T. Gomes*[a]

[a] Centro de Química Estrutural, Institute of Molecular Sciences, Departamento de Engenharia Química, Instituto Superior Técnico, Universidade de Lisboa, Av. Rovisco Pais 1, 1049-001 Lisboa, Portugal. E-mail: pedro.t.gomes@tecnico.ulisboa.pt

[b] Centro de Ciências e Tecnologias Nucleares, Departamento de Engenharia e Ciências Nucleares, Instituto Superior Técnico, Universidade de Lisboa, 2695-066 Bobadela LRS, Portugal. E-mail: lpereira@ctn.tecnico.ulisboa.pt

[c] CFisUC - Centro de Física da Universidade de Coimbra, Departamento de Física, Universidade de Coimbra, Portugal.

[d] BioISI - Biosystems & Integrative Sciences Institute, Departamento de Química e Bioquímica, Faculdade de Ciências, Universidade de Lisboa, Campo Grande, Ed. C8, 1749-016 Lisboa, Portugal. E-mail: nuno.bandeira@fc.ul.pt

[e] Institut für Physikalische Chemie, Universität Stuttgart, Pfaffenwaldring 55, Stuttgart D-70569, Germany. E-mail: slageren@ipc.uni-stuttgart.de

Table of Contents

Experimental section

General Considerations

All operations dealing with air- and/or moisture-sensitive materials were carried out under inert atmosphere using a dual vacuum/nitrogen line, glovebox and standard Schlenk techniques. All solvents used were pre-dried with 4 Å molecular sieves and purified by refluxing over a suitable drying agent followed by distillation under nitrogen. THF was dried over sodium/benzophenone and *n*-hexane over calcium hydride. Solvents and solutions were transferred using a positive pressure of nitrogen through stainless steel cannulas and mixtures were filtered in a similar way using modified cannulas that could be fitted with glass fiber filter disks.

Elemental analyses were performed in a Fisons Instrument Mod EA-1108, at Laboratório de Análises (IST).

FTIR measurements were conducted on a Bruker Alpha II ATR IR spectrometer located inside a glovebox.

Synthesis of complex [Co{κ^2N,N'-5-(2,4,6-iPr$_3$-C$_6$H$_2$)-NC$_4$H$_2$-2-C(H)=N(2,6-iPr$_2$-C$_6$H$_3$)}$_2$] (1)

NaH (0.041 g, 1.7 mmol) was suspended in THF (20 mL) and a THF (20 mL) solution of the ligand precursor 5-(2,4,6-triisopropylphenyl)-2-(N-2,6-diisopropylphenylformimino)pyrrole[1] (0.68 g, 1.5 mmol) was added. The mixture was allowed to stir for 2 hours, at 90 ºC, under nitrogen, yielding a brown-red suspension. After cooling to room temperature, the solution was filtered and added dropwise to a suspension of anhydrous CoCl$_2$ (0.097 g, 0.75 mmol) in THF (10 mL), which was cooled to -80 °C. The mixture was allowed to warm up to room temperature while stirring overnight. All volatiles were evaporated under reduced pressure, and the residue was extracted with *n*-hexane until extracts were colourless. The solution was concentrated and stored at -20 ºC, from which red crystals of **1** suitable for X-ray diffraction were obtained. Yield: 0.42 g (62%).

^{1}H NMR (300 MHz, C$_6$D$_6$) δ 113.64 (br), 44.29 (br), 32.76 (br), 9.47 (br), 4.27 (br), 0.67 (br), -2.05 (br), -4.41 (br), -5.77 (br), -6.14 (br), -6.31 (br), -7.75 (br), -12.85 (br), -17.21 (br), -20.59 (br), -22.85 (br). μ_{eff} (toluene-d_8, r.t.): 5.2 μ_B; μ_{eff} (solid state, r.t.): 4.7 μ_B. FTIR (ATR, cm^{-1}): 1569 (s, C=N). *Anal.* Calc. for C$_{50}$H$_{66}$CoN$_4$: C, 79.22; H, 8.93; N, 5.77. Found: C, 79.10; H, 9.37; N, 5.80.

^{1}H NMR spectrum
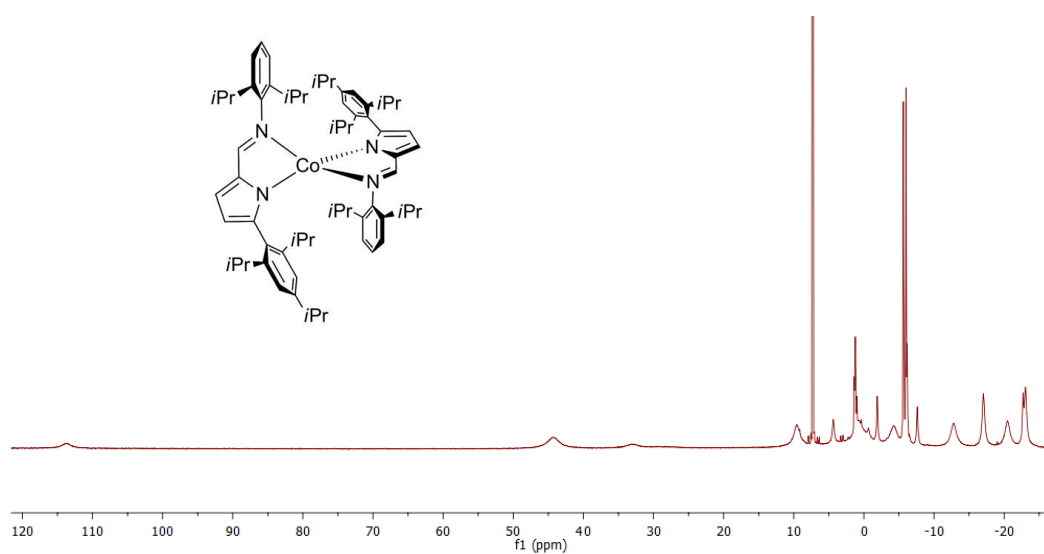
Figure S1 ^{1}H NMR spectrum (300 MHz, C$_6$D$_6$) of **1**.

FTIR spectrum
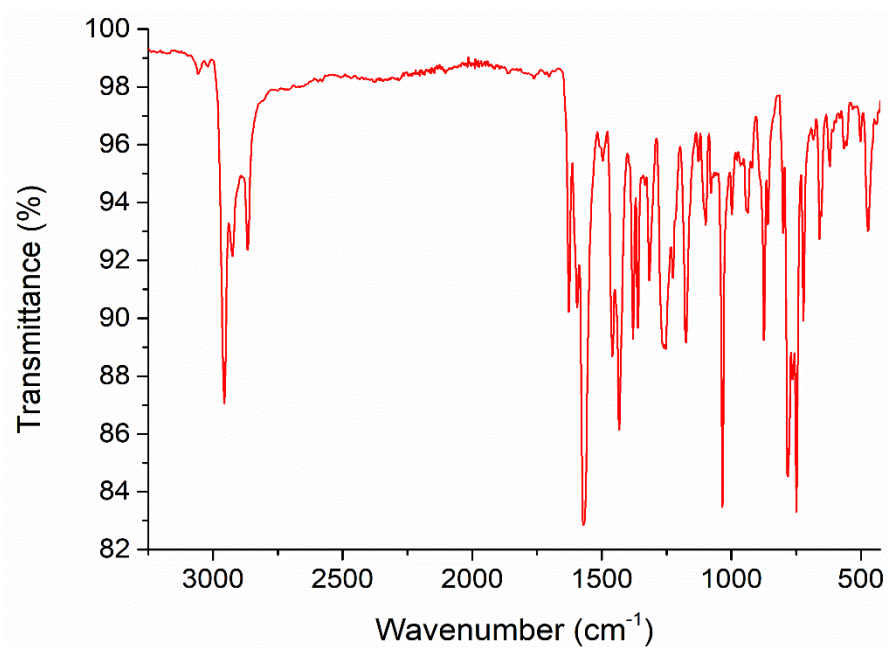
Figure S2 FTIR spectrum of complex **1**.

Nuclear Magnetic Resonance (NMR) measurements

The NMR spectrum of complex **1** was recorded on a Bruker Avance III 300 (^{1}H, 300.130 MHz; ^{13}C, 75.468 MHz) spectrometer. The spectrum was referenced internally using the residual protio-solvent (^{1}H), being reported relative to tetramethylsilane ($\delta = 0$). Complex **1** was dissolved in degassed and dried C_6D_6, being the solution prepared in a J. Young tube, in a glovebox. The deuterated solvents were dried over activated 4 Å molecular sieves and degassed by the freeze-pump-thaw technique. All resonances were characterized by their chemical shifts (δ), quoted in ppm and the multiplicities were abbreviated as broad (br).

The magnetic susceptibility measurement in solution was performed on a Bruker AVANCE III 300 MHz spectrometer at 298 K using the Evans method,[2] the solution sample being prepared in toluene-d_8 with 3% hexamethyldisiloxane, inside a dinitrogen filled glovebox, and transferred to a J. Young NMR tube containing a capillary tube filled with the same solvent mixture, in which hexamethyldisiloxane is the external reference.

Single crystal X-ray diffraction

Single crystals of **1** were covered with polyfluoroether oil, selected under an inert atmosphere, and mounted on a nylon loop. The crystallographic data were collected using graphite monochromated Mo-Kα radiation (λ=0.71073 Å) on a Bruker AXS-KAPPA APEX II diffractometer equipped with an Oxford Cryosystem open-flow nitrogen cryostat, at 150 K. Cell parameters were retrieved using Bruker SMART software and refined using Bruker SAINT[3] on all observed reflections. Absorption corrections were applied using SADABS.[4] Structure solution and refinement were performed using direct methods with the programs SIR2014[5] and SHELXL[6] included in the package of programs WINGX-Version 2014.1.[7] All non-hydrogen atoms were refined anisotropically and the hydrogen atoms were inserted in idealized positions and refined as riding on the parent carbon atom. All the structures refined to a perfect convergence. The graphic presentation was generated using ORTEP-3,[8] where ellipsoids were drawn with a 30% probability, and the hydrogen atoms were omitted for clarity; Mercury 2020.3.0 software was used for the generation of the spacefill representation in Figure S3. Data for complex **1** was deposited in CCDC under the deposit number 2179439.

Table S1 Selected bond distances (Å) and bond angles (°), θ, ф, and ω angles and parameters τ_4 for complex **1**.

Distances (Å)	
Co-N1	1.999(3)
Co-N2	2.034(4)
Co-N3	2.004(4)
Co-N4	2.036(4)
Angles (°)	
N1-Co-N3	118.72(14)
N2-Co-N4	124.82(15)
N1-Co-N4	122.35(15)
N3-Co-N2	126.98(15)
N1-Co-N2 (θ_1) [a]	84.43(15)
N3-Co-N4 (θ_2) [a]	84.38(15)
Angle ф [b]	87.32(15)
Angle ω [c]	163.69(9)
Parameter τ_4 [d]	0.77

[a] θ_1 and θ_2 = N-Co-N chelating ligands bite angles; [b] ф = dihedral angle formed between planes defined by atoms (Co, N1, N2) and (Co, N3, N4); [c] ω = interligand angle formed between dummy bonds Co-centroid (C2-C6) and Co-centroid (C34-C38); [d] Ref. 9
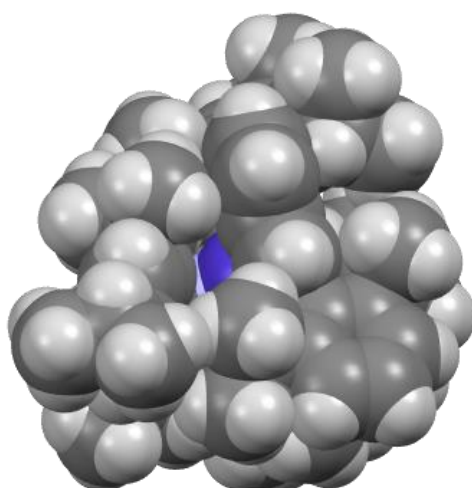
Figure S3 Spacefill view of the X-ray molecular structure of complex **1**, showing the stereochemical protection of the Co(II) metal centre.

Table S2 Crystallographic data for complex **1**.

Formula	$C_{64}H_{86}CoN_4$
M	970.29
λ (Å)	0.71073
T (K)	150(2)
Crystal system	Monoclinic
Space group	$P\,2_1/c$
a (Å)	12.9181(10)
b (Å)	23.922(2)
c (Å)	18.3733(14)
α (Å)	90
β (Å)	96.868(3)
γ (Å)	90
V (Å^3)	5637.2(8)
Z	4
ρ_{calc} (g.cm^{-3})	1.143
μ (mm^{-1})	0.346
Crystal size	0.200×0.140×0.100
Crystal colour	Red
Crystal description	Prism
θ_{max} (º)	25.714
Total data	31313
Unique data	10672
R_{int}	0.1894
$R\,[I > 2s(I)]$	0.0720
R_w	0.1365
Goodness of fit	0.934

HFEPR details

The spectra were recorded at 320 GHz, 0-15 T and 50-120 K on a home-built spectrometer consisting of a VDI signal generator, VDI broadband frequency multipliers, a Thomas Keating Ltd. quasioptical bridge and probe, and a QMC Instruments InSb bolometer detector.[10] The samples were mounted in a 15 T Oxford Instruments helium bath magnetocryostat. The external field is modulated at kHz frequencies to allow for lock-in detection.

Computational details

The ORCA program[11] package version 5.0.3 was used for all the property calculations using the structures derived from single-crystal X-ray diffraction as input. The N-Electron Valence perturbational method[12,13] to second order was employed with the Resolution of Identity[14] (RI-NEVPT2) approximation. The Complete Active Space Self-Consistent Field (CASSCF)[15] wavefunction was determined in the full configuration interaction (CI) space as the state-average of 10 quartets and 40 doublets (seven electrons in five 3d orbitals). The single state perturbed NEVPT2 wavefunctions underwent a multi-state extension to quasi-degenerate NEVPT2 (QD-NEVPT2)[16] in the Nakano[17] formulation.

The exchange integrals were calculated through the RI[18] density fitting technique. The Douglas-Kroll-Hess[19–21] scalar relativistic Hamiltonian truncated to second order (DKH2) was applied with the correspondingly contracted triple zeta doubly polarized basis sets (DKH-TZVPP) for cobalt, for nitrogen DKH-TZVP, and for C and H a split-valence basis set (DKH-SV(P)). The density fitting auxiliary basis sets were chosen to be the generic Karlsruhe[22] def2-TZVP/C specific basis set for the treatment of the perturbative RI section.

The anisotropy (D, E) parameters and g values were calculated in the framework of QD-NEVPT2 via the spin-orbit mean field[23,24] formalism using an effective Hamiltonian[25] by projection of the CI matrix onto the model states. The spin orbit states were projected onto the spin Hamiltonian:

$$\hat{H} = \hat{S}\mathbf{D}\hat{S} \tag{S1}$$

$$\hat{H}_{ZFS} = D\hat{S}_z^2 + E(\hat{S}_x^2 - \hat{S}_y^2) \tag{S2}$$

where $\mathbf{D}$ is the zero-field splitting tensor (equation S1) possessing the following scalar parameters in the magnetic axis frame (equation S2): $D=3/2D_{zz}$ and $E=(D_{xx}-D_{yy})/2$. By convention $D_{xx} \geq D_{yy}$ so that E is always positive. If $D<0$ there may be a barrier for magnetization reversal ($-M_s \to +M_s$), whereas for $D>0$ there can be no magnetization reversal and the spin aligns itself in the xy plane.

Computational results

ZFS (cm^{-1})
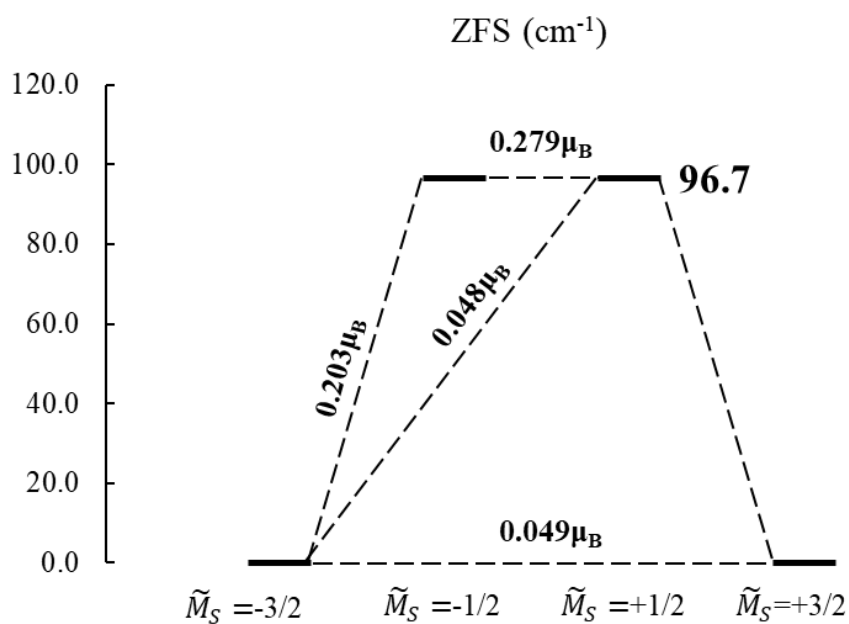
Figure S4 Kramers doublets and zero-field splitting of the title complex with associated transition magnetic moments between each state.
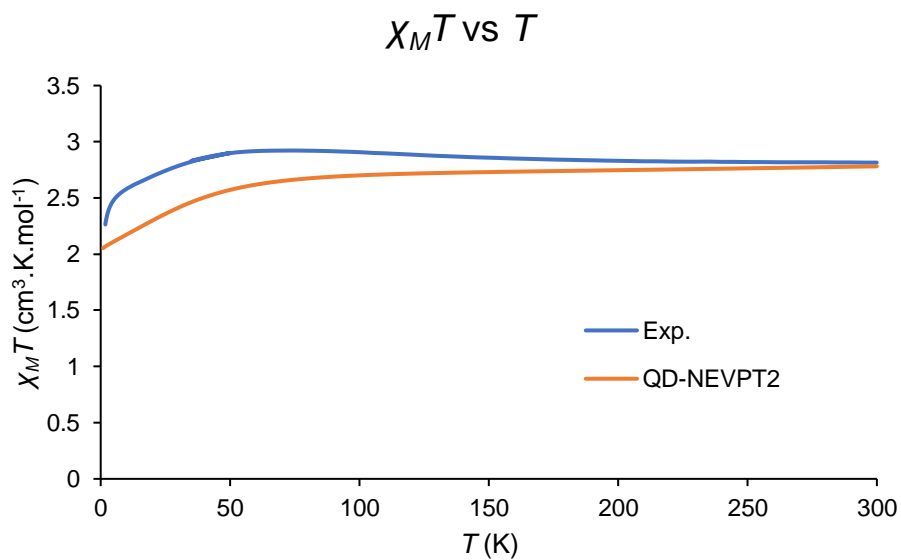
$\chi_M T$ vs T

Figure S5 Experimental and calculated $\chi_M T$ *vs.* T curves ($H = 500$ Oe) of complex **1**.
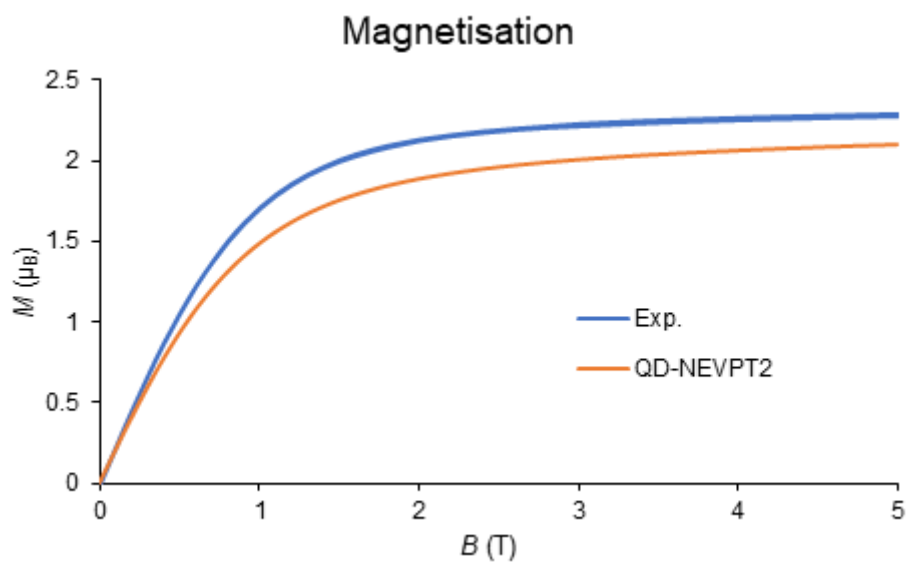
Figure S6 Experimental and calculated magnetisation (M) *vs. B* curves ($T = 1.8$ K) of complex **1**.

Magnetic measurements

A sample of complex **1** (8 mg) was weighed and transferred to the sample holder in a glovebox, due to its air sensitivity.

The static (DC) magnetic measurements were performed using a Quantum Design MPMS3 magnetometer using an applied field of 1000 Oe (0.1 T), from 1.8-50 K, and 10000 Oe (1 T), from 35-300 K. The magnetization curves were obtained from 0 to 7 T at different temperatures (1.8, 5, 10, 20 and 40 K). The measured susceptibility was corrected for diamagnetic and temperature-independent paramagnetic contributions.[26]

The dynamic (AC) magnetic measurements were performed using the ACMS II option of the Quantum Design PPMS (Physical Property Measurement System). The temperature-dependence of the in-phase and out-of-phase components of the AC susceptibility were studied at different frequencies, from 128 up to 5000 Hz, under zero and 1200 Oe applied DC magnetic field, while the frequency-dependent measurements of the AC susceptibility were performed at several different temperatures from 5.5 K to 13.5 K, under zero and 1200 Oe.
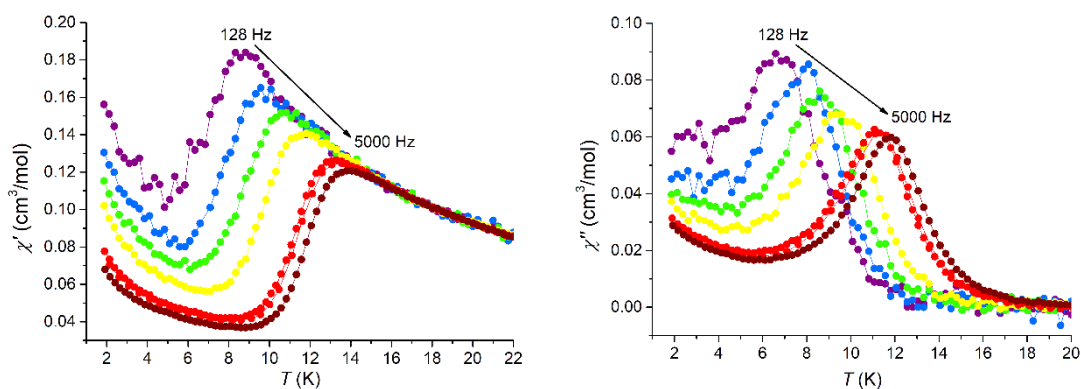
Figure S7 Temperature-dependence of the in-phase, χ' (left) and out-of-phase, χ'' (right) magnetic susceptibilities at several different frequencies in the absence of an external magnetic field.
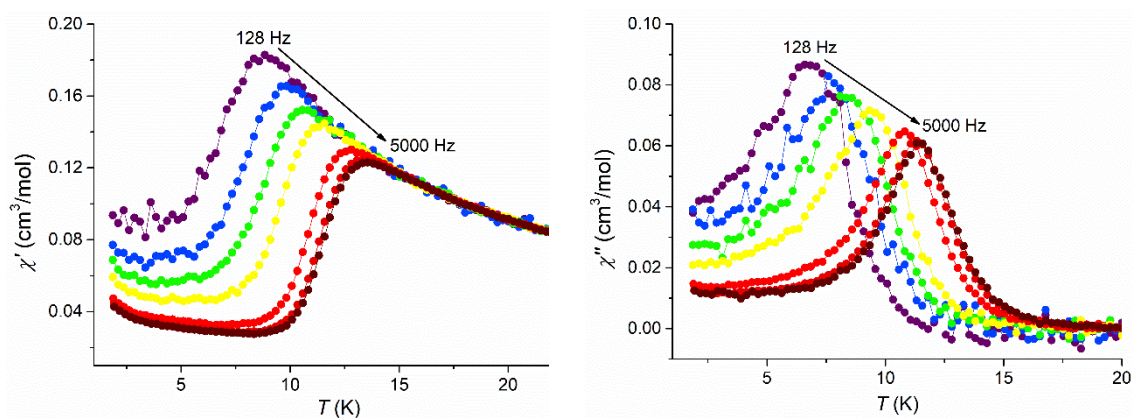
Figure S8 Temperature-dependence of the in-phase, χ' (left) and out-of-phase, χ'' (right) magnetic susceptibilities at several different frequencies under a DC applied magnetic field of 1200 Oe.
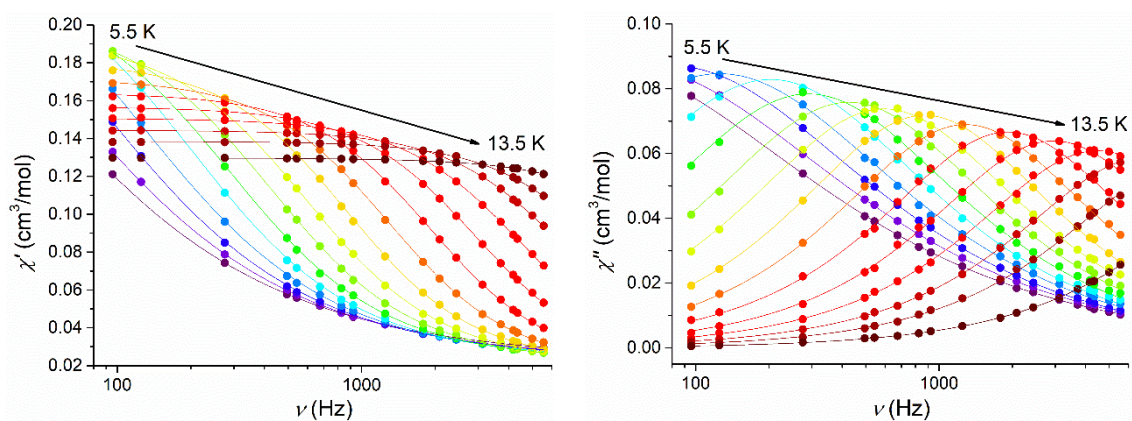
Figure S9 Frequency-dependence of the in-phase, χ' (left) and out-of-phase, χ'' (right) magnetic susceptibilities at several different temperatures for **1** under an applied DC field of 1200 Oe. The solid lines are for guidance.

Table S3 Fitting parameters of the generalized Debye model for complex **1**, from 6 to13.5 K, without the application of a DC field.

T (K)	χ_T (cm^3/mol)	χ_S (cm^3/mol)	τ (s)	α
6	0.328(1)	0.03515(9)	$2.96(3) \times 10^{-3}$	0.299(2)
6.5	0.291(1)	0.0338(1)	$1.82(1) \times 10^{-3}$	0.270(2)
7	0.2652(8)	0.0327(1)	$1.220(9) \times 10^{-3}$	0.230(2)
7.5	0.240(2)	0.0322(4)	$8.2(1) \times 10^{-4}$	0.183(5)
8	0.228(2)	0.0301(7)	$5.7(1) \times 10^{-4}$	0.165(8)
8.5	0.210(2)	0.0288(7)	$4.03(6) \times 10^{-4}$	0.136(8)
9	0.1978(8)	0.0283(5)	$2.87(3) \times 10^{-4}$	0.106(5)
9.5	0.1867(7)	0.0267(5)	$2.06(2) \times 10^{-4}$	0.093(59
10	0.1757(4)	0.0256(4)	$1.434(7) \times 10^{-4}$	0.075(3)
10.5	0.1638(4)	0.0257(5)	$9.96(6) \times 10^{-5}$	0.040(4)
11	0.1587(2)	0.0238(4)	$7.01(3) \times 10^{-5}$	0.045(3)
11.5	0.1514(1)	0.0232(4)	$4.84(2) \times 10^{-5}$	0.029(3)
12	0.1454(1)	0.0224(6)	$3.35(2) \times 10^{-5}$	0.024(3)
12.5	0.13946(9)	0.0240(8)	$2.38(2) \times 10^{-5}$	0.0087(3)
13	0.13478(7)	0.025(1)	$1.69(2) \times 10^{-5}$	0.006(3)
13.5	0.13057(5)	0.025(1)	$1.20(2) \times 10^{-5}$	0.011(3)

Table S4 Fitting parameters of the generalized Debye model for complex **1**, from 5.5 to13.5 K, under an applied DC field of 1200 Oe.

T (K)	χ_T (cm³/mol)	χ_S (cm³/mol)	τ (s)	α
5.5	0.350(3)	0.0223(1)	$4.67(9) \times 10^{-3}$	0.367(2)
6	0.322(2)	0.0217(1)	$3.02(3) \times 10^{-3}$	0.331(1)
6.5	0.297(2)	0.0222(2)	$1.96(3) \times 10^{-3}$	0.282(3)
7	0.273(2)	0.0217(3)	$1.27(2) \times 10^{-3}$	0.245(4)
7.5	0.244(1)	0.0227(4)	$7.8(1) \times 10^{-4}$	0.181(4)
8	0.223(1)	0.0217(4)	$5.48(5) \times 10^{-4}$	0.156(4)
8.5	0.2054(7)	0.0214(3)	$3.74(2) \times 10^{-4}$	0.123(3)
9	0.1944(4)	0.0209(2)	$2.68(1) \times 10^{-4}$	0.103(2)
9.5	0.1814(4)	0.0214(3)	$1.823(7) \times 10^{-4}$	0.069(3)
10	0.1720(3)	0.0199(3)	$1.249(4) \times 10^{-4}$	0.062(2)
10.5	0.1642(3)	0.0199(4)	$8.29(4) \times 10^{-5}$	0.051(3)
11	0.1568(2)	0.0188(5)	$5.39(3) \times 10^{-5}$	0.049(3)
11.5	0.1507(2)	0.0195(7)	$3.55(3) \times 10^{-5}$	0.0479(3)
12	0.14442(7)	0.0200(6)	$2.31(2) \times 10^{-5}$	0.043(2)
12.5	0.1385(1)	0.021(2)	$1.56(3) \times 10^{-5}$	0.032(5)
13.5	0.12975(4)	0.018(3)	$6.7(2) \times 10^{-6}$	0.050(4)
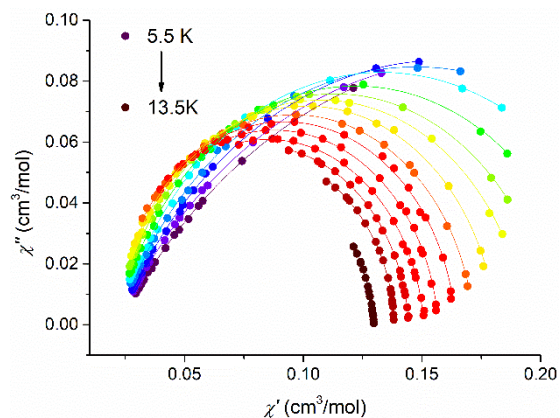
Figure S10 Cole-Cole plots under an applied DC field of 1200 Oe. The solid lines represent the best fits to the experimental data using the generalised Debye model.
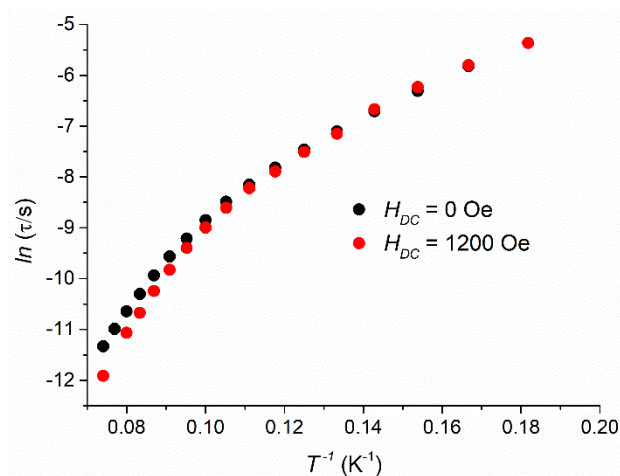
Figure S11 Superposition of both ln(τ) *vs.* T^{-1} plots under $H_{DC} = 0$ Oe (black) and $H_{DC} = 1200$ Oe (red).

References

1. T. F. C. Cruz, P. S. Lopes, L. C. J. Pereira, L. F. Veiros, P. T. Gomes, *Inorg. Chem.* 2018, **57**, 8146–8159.

2. (a) D. F. Evans, *J. Chem. Soc.*, 1959, 2003−2005; (b) S. K. Sur, *J. Magn. Reson.*, 1989, **82**, 169−173.

3. *SAINT Software for the CCD Detector System*, Version 7.03, Bruker AXS Inc., Madison, WI, USA, 2004.

4. G. M. Sheldrick, *SADABS, Program for Empirical Absorption Correction*, Univ. of Göttingen, German, 1996.

5. M. C. Burla, R. Caliandro, B. Carrozzini, G. L. Cascarano, C. Cuocci, C. Giacovazzo, M. Mallamo, A. Mazzone, G. Polidori, *J. Appl. Cryst.*, 2015, **48**, 306–309.

6. (a) G. M. Sheldrick, *Acta Crystallogr.*, 2015, **71**, 3 G. M. Sheldrick, *Acta Crystallogr.*, 2015, **71**, 3–8; (b) C. B. Hübschle, G. M. Sheldrick, B. Dittrich, *J. Appl. Crystallogr.*, 2011, **44**, 1281–1284.

7. (a) L. J. Farrugia, *J. Appl. Crystallogr.,* 1999, **32**, 837–838; (b) L. J. Farrugia, *J. Appl. Crystallogr.*, 2012, **45**, 849–854.

8. (a) M. N. Burnett, C. K. Johnson, *ORTEP-III: Oak Ridge Thermal Ellipsoid Plot Program for Crystal Structure Illustration*, Oak Ridge National Laboratory, 1996, 6895; (b) L. J: Farrugia, *J. Appl. Crystallogr.*, 1997, **30**, 565.

9. L. Yang, D. R. Powell, R. P. Houser, *Dalton Trans*. 2007, 955−964.

10. P. Neugebauer, D. Bloos, R. Marx, P. Lutz, M. Kern, D. Aguilà, J. Vaverka, O. Laguta, C. Dietrich, R. Clérac, J. van Slageren, 2018, **20**, 15528–15534.

11. F. Neese, *WIREs Comput. Mol. Sci*., 2017, **8**, e1327.

12. C. Angeli, R. Cimiraglia, S. Evangelisti, T. Leininger, J.-P. Malrieu, *J. Chem. Phys.*, 2001**, 114**, 10252–10264.

13. C. Angeli, R. Cimiraglia, J.-P Malrieu, *Chem. Phys. Lett*., 2001, **350**, 297–305.

14. O. Vahtras, J. Almlöf, M. W. Feyereisen, *Chem. Phys. Lett*., 1993, **213**, 514–518.

15. B. O. Roos, *The Complete Active Space Self-Consistent Field Method and its Applications in Electronic Structure Calculations*, in *Advances in Chemical Physics,* ed. K. P. Lawley, John Wiley & Sons, Inc., 1987, pp. 399–445.

16. C. Angeli, S. Borini, M. Cestari, R. Cimiraglia, *J. Chem. Phys.*, 2004, **121**, 4043–4049.

17. H. Nakano, *J. Chem. Phys*., 1993, **99**, 7983–7992.

18. S. Kossmann, F. Neese, *Chem. Phys. Lett.*, 2009, **481**, 240–243.

19. B. A. Hess, *Phys. Rev. A*, 1986, **33**, 3742–3748.

20. G. Jansen, B. A. Hess, *Phys. Rev. A*, 1989, **39**, 6016–6017.

21. N. Douglas, N. M. Kroll, *Ann. Phys.*, 1974, **82**, 89–155.

22. A. Hellweg, C. Hättig, S. Höfener, W. Klopper, *Theor. Chem. Acc.*, 2007, **117**, 587–597.

23. B. A. Heß, C. M. Marian, U. Wahlgren, O. Gropen, *Chem. Phys. Lett.*, 1996, **251**, 365–371.

24. F. Neese, *J. Chem. Phys.*, 2005, **122**, 034107.

25. V. Vallet, L. Maron, C. Teichteil, J. P. Flament, *J. Chem. Phys.*, 2000, **113**, 1391–1402.

26. R. L. Carlin, *Magnetochemistry*, Springer, Berlin, 1986.